Sustainable Energy, Grids and Networks 38 (2024) 101355

Contents lists available at ScienceDirect

Sustainable Energy, Grids and Networks

journal homepage: www.elsevier.com/locate/segan

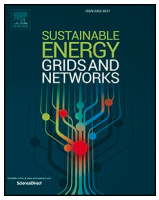

Data-driven approach for the detection of faults in district heating networks

Enzo Losi *, Lucrezia Manservigi, Pier Ruggero Spina, Mauro Venturini

Università degli Studi di Ferrara, Via G. Saragat 1, Ferrara 44122, Italy

ARTICLE INFO

Keywords:
District heating networks
Diagnostics
Fault detection and identification
Neural networks

ABSTRACT

At present, District Heating Networks (DHNs) are required to operate more and more reliably and efficiently in order to further save primary energy and reduce environmental impact. Thus, monitoring and diagnostic approaches are necessary to identify the typical faults that affect this type of systems (e.g., anomalous heat and pressure losses), with the final goal of optimizing DHN operation and management. To this aim, this paper presents a data-driven diagnostic methodology that exploits NARX (nonlinear autoregressive network with exogenous inputs) neural networks to simulate DHN healthy operation and a threshold-based criterion for fault detection and identification. The novel diagnostic methodology is tested for evaluating the health state of the DHN of the campus of the University of Parma (Italy), based on the availability of time series of measurable variables (mass flow rate, pressure, and temperature) for both the power plant and the end-users. Both single and multiple faults of anomalous heat losses and anomalous pressure losses, with different magnitudes and location, were artificially implanted in DHN pipes. The main novel contribution of this paper with respect to state-of-the-art literature relies on the development of a real-time simulation approach aimed to predict DHN future operation and detect abnormal deviations from normal operation. The methodology proves to correctly detect and identify all simulated faults related to heat and pressure losses, by also correctly estimating their magnitude even in the most challenging scenarios.

1. Introduction

1.1. Problem statement

The ambitious target set by the European Union towards climate neutrality motivated the scientific community to develop strategies to reduce greenhouse emissions [1]. This ambitious goal can be addressed by pushing the decarbonization of the residential sector, in which a large part of energy consumption is currently used for space heating [2]. In this framework, District Heating Networks (DHNs) do play an important role [1,3] as users' thermal energy demand is met by using a heat carrier that is heated [4] by a heat source (e.g., combined heat and power plants [2,3], heat pumps and thermal energy storages [5]) and subsequently transported through a distribution network.

DHNs are usually designed to operate for several decades (up to thirty years [6]) and thus their reliability may be compromised by several faults. As an example, we report a list of severe failures that occurred in some DHNs. The DHN of Heilongjiang underwent more than one thousand failures over four years [7,8], while the DHN of Tianjin was affected by thirty-two failures ([6]) over a year. In 2019, a pipe broke in Yinchuan, by reducing the reliability of heating supply [9]. In 2020, heating pipes broke in Harbin and Shandong, by cutting the heating supply to more than ten thousand users [9] and eighty-three heat exchange stations [6], respectively. Finally, the 74% of the 135 substations in two Swedish district heating systems was faulty [10]. In some cases, DHN faults may even remain undetected due to non-effective compensation actions or improper maintenance practice [11]. As a result, heating energy consumption significantly increases, thermal comfort in buildings reduces and, in the worst cases, costumers' health can be threatened [7].

Such catastrophic consequences can be prevented by using automatic diagnostic methodologies for continuously monitoring DHN health state, and promptly detecting and identifying faults.

In the literature, diagnostic methodologies are usually grouped in two classes, i.e., physics-based models and data-driven models. Physics-based models are mature approaches that describe the operation of the system by using several specific parameters [12], e.g., pipe length and diameter, insulation type and thickness, roughness, etc., which can be unknown or not available. Thus, significant modeling efforts are usually required. Conversely, data-driven models do not require an in-depth knowledge of DHN characteristics and can be often applied more

* Corresponding author.
E-mail address: enzo.losi@unife.it (E. Losi).

https://doi.org/10.1016/j.segan.2024.101355
Received 27 October 2023; Received in revised form 18 March 2024; Accepted 18 March 2024
Available online 19 March 2024

Nomenclature

Symbols

b	bias
D	diameter
d	delay
F	mapping function
k	parameter of the fault detection criterion
L	time series length
n	number of data that satisfy the fault detection criterion
N	number of hidden neurons
p	pressure
$\widehat{p}$	predicted pressure
Q	mass flow rate
$\widehat{Q}$	predicted mass flow rate
RMSE	root mean square error
r	residual
S	total number of predictor variables
T	temperature
$\widehat{T}$	predicted temperature
$\boldsymbol{X}$	set of all predictor time series
$\widetilde{\boldsymbol{X}}$	matrix of delayed values of predictor variables
$\boldsymbol{x}$	predictor time series
Y	target time series
y	output variable
$\widetilde{y}$	matrix of delayed values of target variable
$\widehat{y}$	predicted output variable
W	matrix of weights
α	detection rate
Δ	relative variation
ε	pipe roughness
λ	thermal conductivity
σ	standard deviation

Superscripts and subscripts

i	end-user label
I	input layer
j	faulty dataset label
h	hidden layer
ov	overall
PP	power plant
t	time step
ts	test
*	healthy dataset

Acronyms

CA	Closed-loop Architecture
DHN	District Heating Network
EU	End-User
FCA	Fully Closed-loop Architecture
HL	Heat Loss
NARX	Nonlinear autoregressive network with exogenous inputs
OA	Open-loop Architecture
PL	Pressure Loss
PP	Power plant
S	Split node
WL	Water Leakage

directly than physics-based models. On the other hand, the diagnostic response depends on data availability and quality [12]. In fact, data-driven methods correlate system variables (in this paper, flow rate, pressure, and temperature) with DHN faults, thus requiring a regular monitoring activity as well as a preprocessing phase to clean data noise and remove outliers.

The main challenge related to DHN diagnosis relies on the fact that all system components, e.g., valves and actuators, can be subject to malfunctions. To this purpose, some researchers developed both physics-based and data-driven methodologies for the diagnosis of heat exchangers ([13–17]), sensors ([18–21]) and other DHN devices ([22,23]).

DHN reliability can also be compromised by pipe failures, which are caused by physical, environmental, and operational factors and lead to three types of faults, namely leakage, pressure loss and heat loss, of which the causes were reviewed in [24].

The high number of fault causes makes pipe failures much more frequent than those affecting other components ([25]). For example, the 56% of failures occurred in the DHN of Heilongjiang (China) over a year was caused by faulty pipes ([7,8]).

The present paper deals with the diagnostics of faults occurring in DHN pipes. Thus, Section 1.2 documents and discusses the state-of-the-art literature related to this topic, while Section 1.3 discusses benefits and challenges related to the use of data-driven approaches.

1.2. Literature survey on DHN diagnostics

Despite several factors contribute to deteriorate the health state of DHN pipes, the detection and identification of pipe failures is still an open field of research. Some recent studies are documented in the following, by analyzing the three most frequent failures (leakage, heat losses, pressure drops).

For the sake of leakage detection, Rüger et al. [26] proposed a pressure wave-based approach, while Xue et al. [27] exploited a novel machine-learning approach. In Hossain et al. [28], infrared images were analyzed by means of a convolutional neural network and eight classifiers (e.g., decision tree and support vector machine) to assess the most reliable data-driven model for leakage detection. Fan et al. [29] designed a two-level diagnostic model that was able to assess the leakage position by using a deep belief network. Finally, Zhou et al. [30] identified leakage location by means of back propagation neural networks.

The studies [23,31–39] focused on heat loss evaluation and detection and are thus briefly reviewed in the following one by one. Li et al. [23] exploited a convolutional neural network to identify the pipes affected by anomalous heat losses. Nowak-Ocłoń and Ocłoń [31] assessed the influence of different insulation materials on heat losses. The same goal was pursued in Chicherin et al. [32] by means of a data-driven approach. Danielewicz et al. [33] proposed a three-dimensional numerical model that calculated heat losses of DHN pipelines. Zheng et al. [34] developed a thermo-hydraulic model to simulate the operation of the DHN of Tianjin. The model designed by Fang and Lahdelma [35] used meter readings to calculate heat losses, while Lidén et al. ([36,37]) showed that drainage valves could be used to evaluate the thermal health state of DHN pipes. Wang et al. [38] exploited a genetic algorithm to assess the deterioration of pipe insulation. Keçebaş and Yabanova [39] monitored the thermal efficiency of a DHN by using a multi-layer perceptron.

Finally, with regard to the estimation of ordinary pressure drops within DHN pipes, the models developed in [27,34,35,38], used balance equations. However, to the authors' knowledge, no study was specifically tuned for detecting *anomalous* pressure loss within DHNs, with the exception of the study conducted by Kaltenbacher et al. [40].

The literature survey documented above points out that most diagnostic methodologies were specifically tuned to identify one fault type at a time. Thus, a comprehensive approach that simultaneously detects and identifies leakage, anomalous pressure losses and heat losses still lacks.

This goal was pursued by Manservigi et al. ([24]) and Bahlawan et al. ([41,42]), who developed a novel diagnostic methodology that coupled a physics-based modeling approach with an optimization algorithm to identify the health state of all DHN pipes for all the above-mentioned pipe faults. Despite the extremely positive results documented in [24, 41,42], the application of the novel physics-based diagnostic methodology may be awkward as several pipe characteristics, e.g., length and roughness, have to be known [24]. In fact, such pieces of information may not always be available or may vary over time, by making the diagnosis untrustworthy. In addition, the diagnostic methodology assesses pipe health state under steady-state conditions, whereas DHNs usually operate under transient conditions because of frequent start-ups and shut-downs [43].

The drawbacks of the physics-based diagnostic methodology developed in [24,41,42] can be overcome by designing a comprehensive methodology composed of two diagnostic steps. A data-driven model, which is the goal of this paper, is employed for a first assessment of DHN health state under both steady-state and transient conditions, thanks to the fact that it does not require an in-depth knowledge of DHN characteristic. Then, when candidate faults are detected, a physics-based diagnostic methodology (e.g., the one developed in [24,41,42]) carries out an accurate evaluation of the faulty pipes, by identifying the fault type and magnitude under steady-state conditions.

1.3. Benefits and challenges of data-driven approaches

In the last ten years, the advancements in information technology, big data analytics, and artificial intelligence together with the capability of enterprises to generate massive volumes of data have sparked the interest in implementing data-driven methodologies.

These methodologies usually comprise several steps for collecting, processing, and analyzing data, in order to support the decision-making process [44]. For example, in the field of energy systems, data-driven methodologies have been developed for the diagnostics and prognostics of the health state of an asset (e.g., gas turbines [45,46], heat pumps [47], district heating systems [48–50], etc.) to better manage maintenance activity and thus optimize asset operation and efficiency. They utilize historical data that describe the past behavior of a given asset to train a data-driven model, which allows the estimation of current and future health state of the considered asset.

There are several benefits related to the implementation of data-driven methodologies [51]: autonomous learning of non-linear correlations between monitored variables and system health state, capability of handling heterogeneous data, and proven accuracy, thus leading to increased efficiency in decision making and process automation, as well as saving of money and time. Moreover, data-driven models are usually scalable, i.e., they can be retrained once new data are acquired, and suitable to transfer learning. This means that a model developed for a given DHN can be employed for the diagnostics of a similar DHN with minor adjustments.

On the other hand, according to [44] and [51], several challenges must be tackled to successfully implement data-driven methodologies. The first challenge is related to data collection, storage, and management. The second challenge to ensure the development of a reliable model deals with data quality, since the available data must not contain missing values and must well describe the task under analysis (i.e., proper measured variables and time frames must be considered). The proper tool/algorithm (e.g., artificial neural network, support vector machine, decision tree, etc.) to process the data must be identified [21] as well as its optimal tuning has to be investigated. Moreover, the definition of relevant and effective metrics is fundamental to assess the accuracy of the data-driven methodology and allow its improvement over time. Finally, it has to be mentioned that becoming a data-driven organization requires a fundamental change in culture, habits, and mindset of employees to adopt new work methodologies, technologies, and tools [51].

In this framework, we investigate the potential of developing a data-driven methodology for the diagnostics of faults occurring in DHN pipes. The novelty of the proposed methodology is outlined in the next section.

1.4. Novelty and contribution of the paper

This paper proposes a novel data-driven methodology capable of assessing DHN health state. First, the NARX (nonlinear autoregressive network with exogenous inputs) network is trained to reproduce the relationship among DHN parameters under healthy conditions, for both steady-state and transient operation. Then, the same NARX network is used for the real-time diagnosis of potential faults by evaluating the deviation between actual data and NARX predictions. Thus, the proposed approach is mainly aimed at localizing the faulty pipe and can also estimate fault type and magnitude.

The novel diagnostic method is validated by using several faulty datasets generated by means of a digital twin of the DHN of the campus of the University of Parma, which is used in this paper as the case study. The simulated datasets cover different faults occurring in DHN pipes with a different type, magnitude, and location, in order to comprehensively challenge the diagnostic method.

With respect to state-of-the-art literature, the novelty of this paper can be summarized as follows:

- development of a data-driven method for DHN diagnostics that exploits a NARX network to extract the healthy pattern of the DHN as well as its dynamics. Robust fault detection and isolation is obtained by means of a fault criterion that evaluates the deviations from the healthy condition. Such a method is developed for the first time in the literature for DHN diagnostics;
- development of an innovative real-time simulation approach, named “fully-closed architecture” in this paper, which only uses self-generated data to predict the future operation of the DHN, in order to overcome the limitations of standard approaches used for DHN diagnostics by means of neural networks;
- test of the methodology to detect and identify both single faults (i.e., only one pipe is faulty, and the fault cause is unique) and multiple faults (i.e., the fault is triggered by multiple causes). The diagnosis of multiple faults affecting a DHN has been rarely investigated in the literature.

Finally, it must be observed that unlike the study [52], which focused on the detection of fouling in heat exchangers of district heating substations, and the studies [50] and [53], which considered faults occurring in DHN components, the present paper deals with the detection and identification of faults that affect DHN pipes.

1.5. Organization of the paper

The paper is organized as follows. Section 2 presents the diagnostic method, by both discussing its rationale and defining the diagnostic approaches. Moreover, some basics about NARX networks are also provided. Section 3 presents the case study and describes the implanted faults. Section 4 reports the setting of the NARX network and presents the results of the diagnosis of the considered faults. Finally, Conclusions are drawn in Section 5.

2. Methodology

2.1. Overview

The diagnostic method proposed in this paper is composed of two phases, as shown in Fig. 1. The first phase (left hand-side of Fig. 1) is the development of a data-driven model capable of simulating the dynamic behavior of a healthy DHN. Thus, this prediction model is trained on *healthy* data only, i.e., the data representing the healthy operation of the

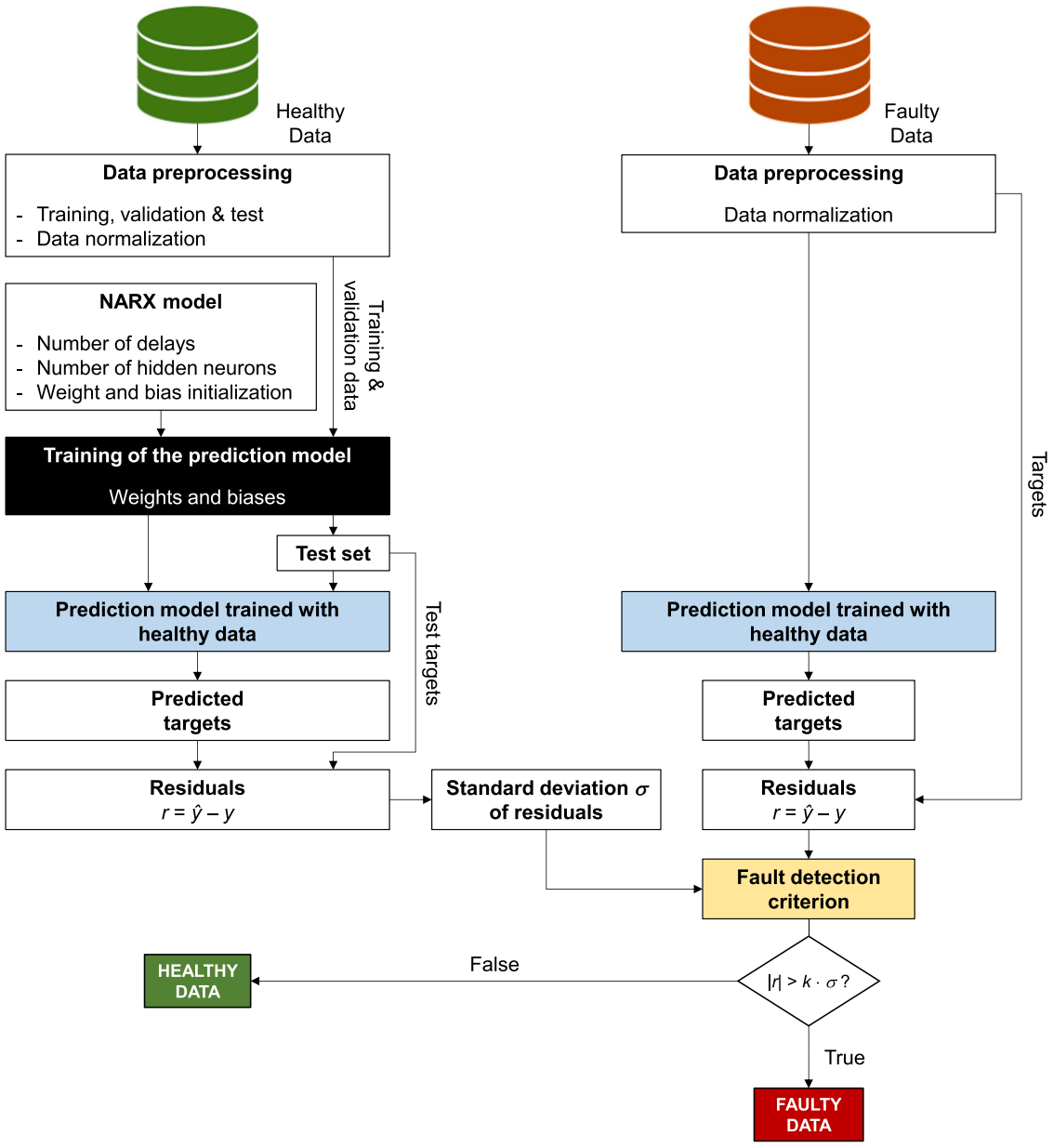

Fig. 1. Diagnostic method.

DHN, to learn the hidden relationship between the power plant (PP) and each end-user (EU). Subsequently, the prediction model is tested on new healthy data to assess its prediction reliability and the standard deviation of the residuals is evaluated to tune the fault detection criterion. The second phase (right hand-side of Fig. 1) consists of employing the previously-trained prediction model for the real-time prediction of the measurable variables of each EU. The k-σ rule is used to detect DHN faults by comparing the actual data of the DHN to those provided by the prediction model.

2.2. NARX neural network

Given the dynamic behavior of a DHN, the target variable at a future time step can be predicted by accounting for the delayed values (i.e., evaluated at antecedent time steps) of the target variable itself and the predictor variables.

By considering S ($S \geq 1$) predictor time series and one target time series composed of L time dependent data points (i.e., the elements of a given time series), we denote with $\boldsymbol{x}^s = (x_1^s, x_2^s, \ldots, x_L^s) \in \mathbb{R}^L$ the s-th predictor time series and we use $\boldsymbol{X} = (\boldsymbol{x}^1, \boldsymbol{x}^2, \ldots, \boldsymbol{x}^S)$ to represent all the predictor time series. The target time series is denoted as $\boldsymbol{Y} = (y_1, y_2, \ldots, y_L) \in \mathbb{R}^L$.

The goal is the prediction of the target variable at the next time step as a function of d previous values of the target series and S predictor (independent) variables, as in Eq. (1):

$$\hat{y}_t = F(y_{t-1}, \ldots, y_{t-d}, \boldsymbol{X}_{t-1}, \ldots, \boldsymbol{X}_{t-d}) \tag{1}$$

where F is the mapping function.

In this paper, a NARX neural network, which is a widely used and powerful tool for time-series modeling [54], is employed for the identification of the mapping function F. A NARX neural network is capable of modeling the dynamic behavior of the DHN, by considering a delay for both predictor and target variables. Eq. (2) specifies the non-linear dependency embedded in the NARX neural network considered in this paper:

$$\hat{y}_t = W_h\left[\text{tansig}(W_I^1 \tilde{\boldsymbol{X}} + W_I^2 \tilde{\boldsymbol{y}}) + b_I\right] + b_h \tag{2}$$

where $\tilde{X} = (x^1_{t-d}, \ldots, x^1_{t-1}, \ldots, x^n_{t-d}, \ldots, x^n_{t-1}) \in \mathbb{R}^{n \cdot d}$ is the matrix containing the delayed values of the predictor variables, $\tilde{y} = (y_{t-1}, \ldots, y_{t-d}) \in \mathbb{R}^d$ is the vector containing the delayed values of the target variable; $W^1_{\mathrm{I}} \in \mathbb{R}^{N \times (n \cdot d)}$, $W^2_{\mathrm{I}} \in \mathbb{R}^{N \times d}$, $W_{\mathrm{h}} \in \mathbb{R}^N$ are the matrices of weights, where N is the number of hidden neurons, and b_{I} and b_{h} are the biases. Finally, *tansig* is the activation function for the hidden layer. The NARX neural networks considered in this work all have one hidden layer.

In this paper, the NARX neural network is trained by means of Bayesian regularization backpropagation and the maximum number of training epochs is 10^3. To improve network generalization, an early stopping criterion is used during training. A validation dataset is considered, and the validation error is monitored during the training process. When the validation error increases for a specified number of consecutive epochs (six in this paper), the training process is stopped, and the weights and biases calculated at the epoch with the minimum validation error are saved.

2.3. Prediction model

As shown in detail in Section 3, a DHN is usually composed of a PP and multiple EUs. Both the PP and each EU are equipped with flow rate meter, pressure sensors, and temperature sensors. Thus, three measurable variables are available, namely flow rate Q, pressure p, and temperature T, for both the PP and each EU.

In this work, each measurable variable of the EU is, in turn, considered as the target variable, while the remaining measurable variables and the ones of the PP are employed as predictor variables. Therefore, for each EU three simulation models are developed, one for each measurable variable according to Eq. (1). The specifications of the three models are reported in Table 1.

This paper investigates three different architectures of the NARX neural network, namely *open*-loop architecture (OA), *closed*-loop architecture (CA), and *fully-closed*-loop architecture (FCA). Both OA and CA are commonly used for training a NARX neural network to simulate real-time operation of a dynamic system [54]. Instead, FCA represents a novel approach, which, in this paper, will demonstrate its superiority with respect to both OA and CA for diagnostic purposes.

The OA is performed as in Eq. (1). All the inputs, i.e., the delayed values of both predictors and target, are "true" values.

In the CA, the estimated output is fed back to the input of the NARX network to predict multiple time steps over time, as reported in Eq. (3), which is derived from Eq. (1) by substituting the "true" delayed values of the target with self-generated data points at the antecedent time steps:

$$\hat{y}_t = F(\hat{y}_{t-1}, \ldots, \hat{y}_{t-d}, \boldsymbol{X}_{t-1}, \ldots, \boldsymbol{X}_{t-d}) \tag{3}$$

It has to be noted that, for this network architecture, all the predictor variables (i.e., $\boldsymbol{X}$, which includes both the variables of the PP and the EU) are fed with the "true" values at each time step.

Instead of the "true" values, the FCA exploits the estimated values (i.e., predicted by the NARX network itself) also for predictor variables of the EUs, while the "true" values are employed only for the variables of the PP.

The FCA developed in this paper is shown in Fig. 2 and is defined in Eqs. (4) - (6), which are also derived from Eq. (1):

$$\hat{Q}_t = F_Q(\hat{Q}_{t-1}, \ldots, \hat{Q}_{t-d}, \hat{p}_{t-1}, \ldots, \hat{p}_{t-d}, \hat{T}_{t-1}, \ldots, \hat{T}_{t-d}, \boldsymbol{X}^{\mathrm{PP}}_{t-1}, \ldots, \boldsymbol{X}^{\mathrm{PP}}_{t-d}) \tag{4}$$

$$\hat{p}_t = F_p(\hat{p}_{t-1}, \ldots, \hat{p}_{t-d}, \hat{Q}_{t-1}, \ldots, \hat{Q}_{t-d}, \hat{T}_{t-1}, \ldots, \hat{T}_{t-d}, \boldsymbol{X}^{\mathrm{PP}}_{t-1}, \ldots, \boldsymbol{X}^{\mathrm{PP}}_{t-d}) \tag{5}$$

$$\hat{T}_t = F_T(\hat{T}_{t-1}, \ldots, \hat{T}_{t-\mathrm{d}}, \hat{Q}_{t-1}, \ldots, \hat{Q}_{t-d}, \hat{p}_{t-1}, \ldots, \hat{p}_{t-d}, \boldsymbol{X}^{\mathrm{PP}}_{t-1}, \ldots, \boldsymbol{X}^{\mathrm{PP}}_{t-d}) \tag{6}$$

where $\boldsymbol{X}^{\mathrm{PP}}$ contains the "true" values of the variables of the PP.

At each time step t, the three simulation models are run simultaneously one step at a time, and the delayed predicted values of each variable are fed back to the input of all models. Thus, the FCA is designed in order to reduce the influence of a potential fault on the prediction of the target variables. In this manner, the FCA mimics a healthy DHN and thus maximizes the diagnostic capability of the proposed methodology.

Such an approach is developed only for the sake of diagnosing DHN health state, while, by nature, OA and CA are used for reproducing the DHN behavior under healthy conditions.

In summary, all the three architectures implement the same transfer function, i.e., Eq. (1), but an increasing amount of self-generated inputs is used to predict the output passing from OA to CA and then to FCA. More in detail, the variables related to the PP are always fed as "true" values for all the three architectures, while all the variables related to each EU (three for each end-user) can be "true" values (OA) or self-generated values (CA and FCA). Among all the inputs, in the CA architecture, only the delayed values of the target variable are self-generated, while all the three variables related to each EU are self-generated in the FCA architecture.

2.4. Fault detection criterion

The diagnostic method proposed in this paper employs the k-σ rule for anomaly detection. After training, the prediction model is tested on unseen healthy data to assess its prediction reliability and tune the fault detection criterion. The distribution of the residuals approximates a Gaussian distribution with zero mean and standard deviation equal to σ [54]. The standard deviation σ of the residuals r on tested (healthy) data is computed as in Eq. (7):

$$\sigma = \frac{1}{L-1} \sum_{l=1}^{L} (r_l - \bar{r})^2 \tag{7}$$

where $r = (\hat{y} - y)$ is the difference between the predicted value and the corresponding true value and $\bar{r}$ is the mean of the residuals.

The fault detection criterion adopted in this paper is defined in Eq. (8):

$$|r| > k \cdot \sigma \tag{8}$$

In this paper, k is set equal to 3; thus, the fault detection thresholds are equal to $]-3\sigma, 3\sigma[$. Consequently, the probability of residuals of healthy data to exceed the range $]-3\sigma, 3\sigma]$ is as low as 0.27%. According to Eq. (8), if the absolute value of the residual does not exceed 3σ, then a given data point is labeled as healthy; otherwise, it is labeled as faulty.

Table 1
NARX model variables (Q: mass flow rate; p: pressure; T: temperature; PP: power plant).

Model	Predictors	Target	Inputs	Output
Q	p_i, T_i, Q_{PP}, p_{PP}, T_{PP}	Q_i	$\{Q_{i,\,t-1}, \ldots, Q_{i,\,t-d}, p_{i,\,t-1}, \ldots, p_{i,\,t-d}, T_{i,\,t-1}, \ldots, T_{i,\,t-d}, Q_{\mathrm{PP},\,t-1}, \ldots, Q_{\mathrm{PP},\,t-d}, p_{\mathrm{PP},\,t-1}, \ldots, p_{\mathrm{PP},\,t-d}, T_{\mathrm{PP},\,t-1}, \ldots, T_{\mathrm{PP},\,t-d}\}$	$Q_{i,\,t}$
p	Q_i, T_i, Q_{PP}, p_{PP}, T_{PP}	p_i	$\{p_{i,\,t-1}, \ldots, p_{i,\,t-d}, Q_{i,\,t-1}, \ldots, Q_{i,\,t-d}, T_{i,\,t-1}, \ldots, T_{i,\,t-d}, Q_{\mathrm{PP},\,t-1}, \ldots, Q_{\mathrm{PP},\,t-d}, p_{\mathrm{PP},\,t-1}, \ldots, p_{\mathrm{PP},\,t-d}, T_{\mathrm{PP},\,t-1}, \ldots, T_{\mathrm{PP},\,t-d}\}$	$p_{i,\,t}$
T	Q_i, p_i, Q_{PP}, p_{PP}, T_{PP}	T_i	$\{T_{i,\,t-1}, \ldots, T_{i,\,t-d}, Q_{i,\,t-1}, \ldots, Q_{i,\,t-d}, p_{i,\,t-1}, \ldots, p_{i,\,t-d}, Q_{\mathrm{PP},\,t-1}, \ldots, Q_{\mathrm{PP},\,t-d}, p_{\mathrm{PP},\,t-1}, \ldots, p_{\mathrm{PP},\,t-d}, T_{\mathrm{PP},\,t-1}, \ldots, T_{\mathrm{PP},\,t-d}\}$	$T_{i,\,t}$

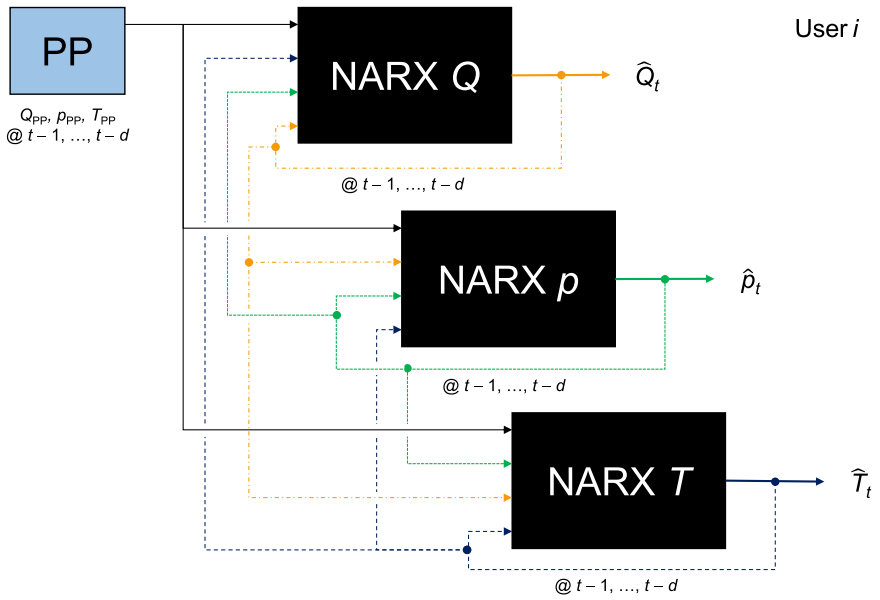

Fig. 2. Fully-closed-loop architecture.

3. Case study

The case study considered in this work is the DHN of the campus of the University of Parma (Italy). The portion of the DHN considered in this paper consists of the supply pipeline that delivers the heat produced by the PP to twelve EUs, which include University departments, laboratories, classrooms, and cafeterias [55]. Fig. 3 illustrates both the actual DHN topology and a simplified scheme. The datasets exploited in this work include EU and PP measurable variables simulated by means of the digital twin presented in [56] and developed in the MATLAB®/Simulink® environment. As demonstrated in [55], such a digital twin provides a detailed and reliable representation of the behavior of the DHN of the campus of the University of Parma, since it accounts for both hydraulic and thermal domains. The exploitation of such simulated datasets is necessary since the validation of a diagnostic tool is usually hindered by the lack of both complex laboratory-scale setups and large-scale labeled datasets (i.e., both the fault and its time of occurrence must be known) [57].

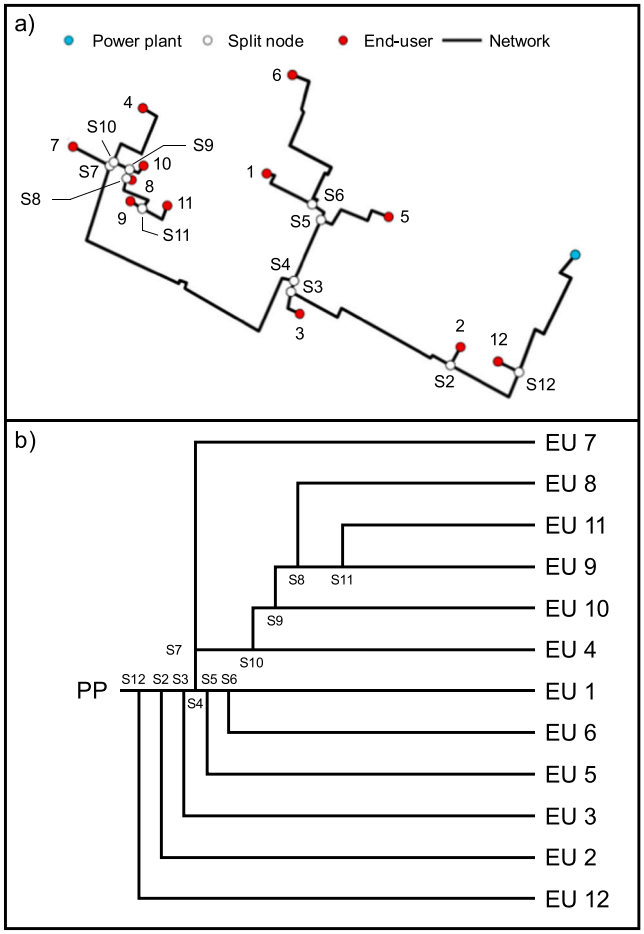

Fig. 3. DNH layout: (a) actual DHN topology; (b) DHN simplified scheme.

3.1. Data description

Ten datasets are considered: one healthy dataset and nine faulty datasets. Each dataset is a collection of time series of measurable variables for both the power plant and the end-users. Ten consecutive days of operation, which mimic DHN operation under both transient and steady-state conditions, are analyzed. The time granularity is equal to one minute, i.e., $L = 14{,}400$ time steps. Each dataset comprises mass flow rate, pressure, and temperature values for both the PP and the EUs. Fig. 4 illustrates the normalized values of mass flow rate, pressure, and temperature at the PP at healthy conditions. Working days (days #1 through #5 and days #8 through #10) are characterized by a similar trend, while Saturday and Sunday (days #6 and #7) follow a different pattern.

The healthy dataset reproduces normal operation of the DHN by assuming that pipes are made of steel and are thermally insulated. The faulty datasets were generated by considering the same boundary conditions (e.g., ground temperature and thermal energy demand of the EUs), but one or more faults were implanted by modifying pipe characteristics, i.e., roughness, thermal conductivity, and internal diameter. The faulty datasets are employed to validate the proposed diagnostic method.

As a final comment, it must be highlighted that the availability of all the considered measurable variables (mass flow rate, pressure, and temperature), for both the power plant and all the end-users, is mandatory for applying the diagnostic methodology presented in this paper. Instead, by considering DHN system dynamics, data sampling

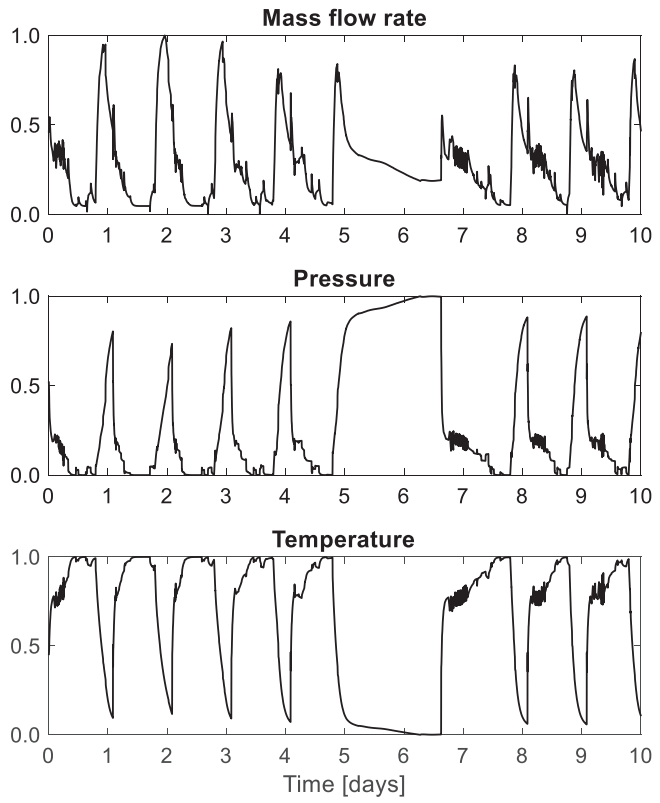

Fig. 4. Normalized values of mass flow rate, pressure, and temperature at the PP at healthy conditions.

frequency can also be lower than the one considered in this paper (i.e., one minute).

3.2. Training and testing

The development of the data-driven prediction model is performed by considering the first seven days of operation, i.e., 10,080 data points of which the 80% are randomly selected and used for training and the remaining 20% are used for validation. For each EU and for each measurable variable, ten different models are trained by using different subsets of data for training and validation. Subsequently, each model is tested on the last three days of each dataset (both healthy dataset and faulty datasets), i.e., 4320 data points.

3.3. Implanted faults

In this paper, three different types of faults are considered, i.e., anomalous heat losses, anomalous pressure losses, and water leakages. The anomalous heat losses were modeled by increasing the thermal conductivity of the insulation layer. To mimic anomalous pressure losses, pipe roughness or internal diameter of the faulty pipe were varied because of pipe fouling or corrosion. Faults that cause anomalous heat and pressure losses can affect the entire length or a portion of the pipe. Finally, two types of water leakage at a different fault location were simulated, i.e., leakages occurring along the pipe and leakages due to a faulty splitting node.

The implanted faults analyzed in this paper are listed in Table 2, where the fault type and location are specified for each faulty dataset as well as the differences with respect to the healthy dataset. Figure A1 in the Appendix highlights the location of the implanted faults.

The faulty datasets are the same employed for the analyses conducted in [41] and [42]. The faults considered in this paper are named as follows: HL for heat losses, PL for pressure losses, and WL for water leakages. Both single (faults HL1, HL2, PL1, PL2, WL1, and WL2) and multiple (faults PL3, PL4, and HL-PL) faults are considered in this paper to validate the diagnostic method. These faults were selected in such a manner that their fault magnitude can be diagnosed, based on the outcomes of the study [24] that investigated the relationship between fault magnitude and the corresponding variation in DHN measurable variables.

The anomalous heat losses of the fault HL1 are caused by the increase of λ_{ins} from 0.04 W m^{-1} K^{-1} to 2.00 W m^{-1} K^{-1} along the entire length of the pipe that connects the splitting node S5 to EU5. Fault HL2 is characterized by anomalous heat losses that concurrently occur in two different pipes: one is the same as in fault HL1 with the same magnitude, and the second faulty pipe is the one that links the splitting nodes S9 and S8. Faults PL1 through PL4 are characterized by anomalous pressure losses caused by an increase of pipe roughness (fault PL1), a reduction of pipe internal diameter (fault PL2), or the simultaneous occurrence of both causes (faults PL3 and PL4). In particular, in fault PL1, the roughness of the faulty pipe, i.e., the pipe bounded by node S5 and EU5, is equal to 1 mm, i.e., ten times its value under healthy conditions. Instead, the anomalous pressure losses simulated in fault PL2 are due to a halved internal diameter of pipe S9-S8 for 10% of pipe length.

Fault PL3 combines the characteristics of faults PL1 and PL2 by simulating the occurrence of both an increase of pipe roughness and a decrease of pipe internal diameter for the pipe that links the splitting nodes S9 and S8. Similarly, fault PL4 considers the same type of fault as in fault PL3 with a further decrease of pipe internal diameter (from D^*_{int} = 0.1000 m to D_{int} = 0.0370 m) and a different location, i.e., pipe S5-EU5.

Table 2
Implanted faults.

Fault	Effect of the fault	Fault location	Faulty parameter	Healthy parameter
HL1	Anomalous heat losses	Entire pipe (S5-EU5)	λ_{ins} = 2.00 W m^{-1} K^{-1}	λ^*_{ins} = 0.04 W m^{-1} K^{-1}
HL2	Anomalous heat losses	Entire pipe (S5-EU5)	λ_{ins} = 0.40 W m^{-1} K^{-1}	λ^*_{ins} = 0.04 W m^{-1} K^{-1}
		Entire pipe (S9-S8)	λ_{ins} = 2.00 W m^{-1} K^{-1}	
PL1	Anomalous pressure losses	Entire pipe (S5-EU5)	ε = 1.0 mm	ε^* = 0.1 mm
PL2	Anomalous pressure losses	10% of pipe length (S9-S8)	D_{int} = 0.0625 m	D^*_{int} = 0.1250 m
PL3	Anomalous pressure losses	Entire pipe (S9-S8)	ε = 1.0 mm	ε^* = 0.1 mm
		10% of pipe length (S9-S8)	D_{int} = 0.0625 m	D^*_{int} = 0.1250 m
PL4	Anomalous pressure losses	Entire pipe (S5-EU5)	ε = 1.0 mm	ε^* = 0.1 mm
		10% of pipe length (S5-EU5)	D_{int} = 0.0370 m	D^*_{int} = 0.1000 m
HL-PL	Anomalous heat losses	Entire pipe (S9-S8)	λ_{ins} = 20.00 W m^{-1} K^{-1}	λ^*_{ins} = 0.04 W m^{-1} K^{-1}
	Anomalous pressure losses	10% of pipe length (S9-S8)	D_{int} = 0.0625 m	D^*_{int} = 0.1250 m
WL1	Water leakages	Node downstream pipe S10-S9	Q_L = 2 kg s^{-1}	No leakage
WL2	Water leakages	Pipe S10-S9	Q_L = 2 kg s^{-1}	No leakage

Fault HL-PL, which affects pipe S9-S8, mimics a multiple fault due to both anomalous heat (λ_{ins} is increased to 20 W m^{-1} K^{-1}) and pressure (pipe diameter is halved) losses.

Finally, faults WL1 and WL2 simulate a water leakage. The leakage in the two faults occurs in a different point, i.e., in the node downstream pipe S10-S9 (fault WL1) or within the pipe S10-S9 (fault WL2). The lost water mass flow rate is the same, i.e., about 2.0% of the water swallowed through the PP.

4. Results and discussion

In this section, the reliability of several NARX configurations (characterized by a different number of delays and/or hidden neurons) is first investigated to identify the optimal set-up of the prediction models as well as the diagnostic method. Then, each faulty dataset listed in Table 2 is analyzed to evaluate the effect of each fault on DHN measurable variables and highlight the EUs that are mostly affected by the implanted faults. This analysis also allows the identification of the faults that can be detected by the diagnostic method. Finally, for each detectable fault, the paper reports the fraction of data that satisfy the fault detection criterion defined in Eq. (8) and the corresponding fault magnitude identified by the diagnostic methodology.

4.1. Prediction model set-up

The paper investigates nine configurations of the NARX model by combining three different values of the delay, $d = \{1, 2, 4\}$, with three values of the number of hidden neurons, $N = \{15, 30, 50\}$. Moreover, for each combination of NARX hyperparameters, ten different subsets are considered for training and validation, by randomly sampling data within the first seven days of the healthy dataset. Thus, for each EU, ninety prediction models are developed in total. Each NARX model is first trained by means of the OA since it allows fast and robust convergence. Subsequently, these models are tested on unseen data (i.e., the last three days of the healthy dataset) by means of both OA and CA.

To identify the optimal set-up of the prediction models, five cases are considered, as defined in Table 3. The different cases consider that the subset used for training and validation and/or NARX configuration are either the same or are different for each variable (Q, p, and T) and/or EU. For example, in case 1, the prediction models for Q, p, and T are trained by means of the same subset and the same configuration is employed for both all variables and EUs; instead, the subset is not necessarily the same for all EUs. Thus, case 1 is the most binding. On the contrary, case 5 allows both subset and NARX configuration to vary for both the variables and EUs.

The metric employed in this paper to evaluate the reliability of each prediction model is the Root Mean Square Error (RMSE), defined in Eq. (9):

$$\mathrm{RMSE} = \sqrt{\frac{1}{L_{ts}} \sum_{l=1}^{L_{ts}} (y_l - \hat{y}_l)^2} \tag{9}$$

where y is the true value, $\hat{y}$ is the prediction of the NARX model, and L_{ts} is the number of tested data points.

Since the three variables have different units of measure and the twelve EUs are characterized by different values of Q, p, and T, the RMSE of each prediction model is calculated by using normalized values (scaled in the range [−1, 1]). An overall RMSE is also calculated, according to Eq. (10), over 3 variables and 12 EUs:

$$\mathrm{RMSE}_{ov} = \sqrt{\frac{1}{3 \cdot 12} \sum_{s=1}^{3} \sum_{j=1}^{12} \mathrm{RMSE}_{sj}^2} \tag{10}$$

It has to be highlighted that, by adopting the OA, for a given configuration of the NARX model, the RMSE on unseen data (not reported in this paper for the sake of brevity) is almost the same by varying the subset (ten in total) used for training and validation. In fact, the variation in the RMSE among the ten prediction models (one per each subset) is about 2%, regardless of the considered delay and number of hidden neurons. Moreover, the prediction models trained by means of different delays and/or number of hidden neurons also perform comparably on unseen data with OA. Consequently, the values of overall RMSE with OA obtained in the five cases are comparable and approximately equal to 0.01.

Therefore, since no rule of thumb can be derived from the results obtained with OA, the optimal setting of each prediction model has to be identified by adopting the CA. Moreover, as it will be demonstrated later in the paper, CA and FCA are more suitable than OA for diagnostic purposes, thus justifying the adoption of CA to select the optimal prediction model for each EU and variable.

Fig. 5 reports the overall RMSE for the five cases (see Table 3) when CA is used for NARX training. Case 5 allows the identification of the best prediction model, i.e., the one characterized by the lowest RMSE among the ninety prediction models, for each variable and EU. The decrease of RMSE by passing from case 1 to case 5 is up to 60%, depending on the considered EU. The overall RMSE obtained in case 5 is equal to 0.11. Instead, the overall RMSE obtained in case 1 is equal to 0.15, and is the highest value obtained among the five cases. The RMSE decreases more significantly by passing from case 2 to case 4 than from case 4 to case 5. This means that model configuration (optimal d and N) more heavily depends on the considered EU, while, for a given EU, a change of model configuration has lower effect on the overall reliability.

Table 4 reports the delay and the number of hidden neurons of the prediction model identified in case 5 for each measurable variable and EU. Such setups apply to OA, CA, and FCA when used for diagnostic purposes. It can be grasped that a delay equal to 4 is usually preferable (18 models out of 36), in particular for the prediction of temperature T, while a delay equal to 1 proves preferable just for a few prediction models. With regard to the number of hidden neurons N, Table 4 proves that a higher value of N is preferable for T (i.e., 30 or 50), while the prediction of Q and p is less influenced by the number of hidden neurons.

Table 3
Cases considered for model set-up ("=" means "same"; "○" means "different").

	Case 1		Case 2		Case 3		Case 4		Case 5	
	Q, p, T	*EU*	*Q, p, T*	*EU*	*Q, p, T*	*EU*	*Q, p, T*	*EU*	*Q, p, T*	*EU*
Subset	=	○	○	○	=	○	○	○	○	○
Config.	=	=	=	=	=	○	=	○	○	○

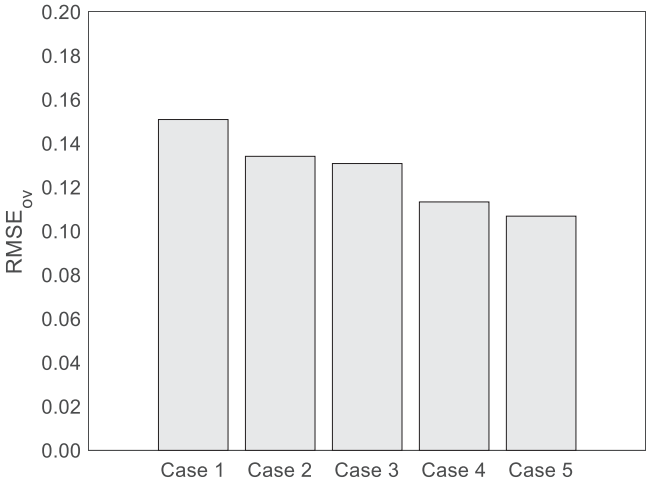

Fig. 5. Overall RMSE on healthy data with CA.

Table 4
Optimal set-up of the prediction models.

End-user	NARX network setting					
	Number of delays			*Number of hidden neurons*		
	Q	p	T	Q	p	T
1	2	1	4	15	15	30
2	2	4	1	50	15	50
3	2	4	2	50	30	50
4	2	2	4	50	50	50
5	1	2	4	15	50	50
6	1	2	4	15	50	30
7	2	2	4	15	15	30
8	4	4	4	15	30	15
9	4	4	4	50	50	50
10	2	2	4	30	15	50
11	4	4	4	50	30	30
12	4	2	2	30	50	50

4.2. Fault's influence on measurable variables

In this section, the measurable variables corresponding to the nine faults are compared to the values under healthy condition for the twelve EUs. This analysis is summarized in Fig. 6, by means of the index Δ defined in Eq. (11):

$$\Delta_{ij} = \frac{y_{ij} - y_i^*}{y_i^*}, \quad y = Q,\ p,\ T \tag{11}$$

where the index i refers to the i-th EU and j to the j-th fault, y^* is the healthy value, and y is the corresponding faulty value. The values reported in Fig. 6 are calculated as the average value over the entire sequence of tested data (4320 data points in total).

Such a preliminary analysis is required as the diagnostic method developed in this paper is data-driven by nature and thus it can only grasp deviations embedded in the measurable variables.

Anomalous heat losses (i.e., faults HL1 and HL2) cause a decrease of the temperature at the inlet of the EU, while they have no effect on variables Q and p. Fault HL1 impacts on the operation of EU5 by decreasing the temperature T of approximately 10%. Thus, fault HL1 can be considered as a "major" fault. The relative variation of variables due to fault HL2 is approximately equal to 2% and the implanted fault affects multiple EUs (i.e., #5, #8, #9, and #11).

Anomalous pressure losses (faults PL1 through PL4) have a direct impact on both Q and p variables. Faults PL1 (single fault) and PL4 (multiple fault) reduce the pressure of EU5 of approximately 1% and 2%, respectively, while mass flow rate shows a decrease equal to 2% and 5%, respectively. In fault PL2, which influences EUs #8, #9, and #11, only 10% of pipe length is affected by a reduction of the internal diameter; thus, fault magnitude is very low on both p (0.2%) and Q (0.5%). Therefore, the diagnostic method is also challenged at detecting and isolating minor faults. Fault PL3 have similar characteristics to fault PL2.

Fault HL-PL combines both anomalous heat and pressure losses. Therefore, the values of all the three variables are affected. In particular, the temperature of EUs #8, #9, and #11 decreases up to 15%; thus, it is the fault with the highest magnitude. Instead, p and Q reduce of approximately 0.2%.

Finally, faults WL1 and WL2 mimic water leakage. It can be noted that they i) significantly affect both Q and p and ii) unlike the other faults, have a direct impact on almost all EUs, though the fault is limited

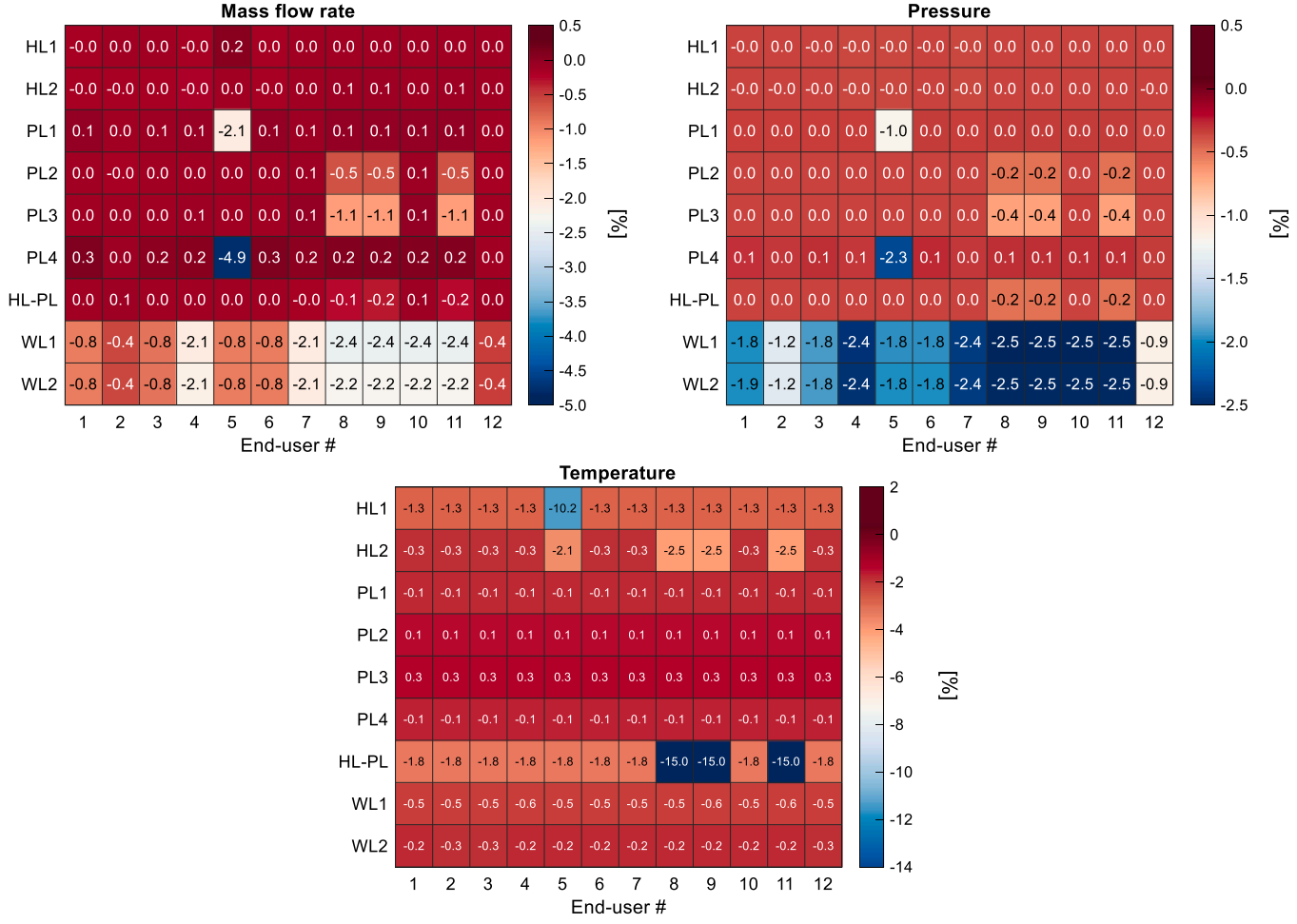

Fig. 6. Relative variation of the three variables due to the implanted faults (faulty value vs. healthy value).

to pipe S10-S9. These two characteristics demonstrate that, by nature, a data-driven approach cannot identify the actual fault location. In fact, the decrease of both Q and p is higher than 2% for EU #4 and EUs #7 through #11, and EUs #1, #3, #5, and #6 are characterized by a reduction of Q and p close to 1% and 2%, respectively. To overcome such issue, before applying the diagnostic method, the balance of mass flow rate between outlet and inlet sections of the power plant should be calculated. If the balance is verified, no leakages occurred in the DHN, and faulty data provided by the diagnostic method on quantities Q and p are caused by anomalous pressure losses along DHN pipes. Otherwise, the DHN is affected by water leakages, but the fault cannot be isolated by the diagnostic method.

In conclusion, the capability of the diagnostic method is investigated by only considering the faults HL1, HL2, PL1 through PL4, and HL-PL. However, it must be observed that these faults comprise both single and multiple faults, as well as minor and major faults, thus challenging the diagnostic method on a wide range of faulty scenarios.

4.3. Assessment of the capability of the diagnostic method

Fig. 7 illustrates the detection rate, α, provided by OA, CA, and FCA for the seven faulty datasets. The metric α, reported in Fig. 7, is calculated according to Eq. (12):

$$\alpha = \frac{n}{L_{ts}} \tag{12}$$

where n is the number of data that satisfy the fault detection criterion defined in Eq. (8) and L_{ts} is the total number of tested faulty data (i.e., 4320 data points in total). It must be noted that the time series data of the implanted faults considered in this paper are not labeled. In fact, a given fault affects most (or even all) measurable variables as well as EUs, as shown in Fig. 6. Thus, the metric α allows the evaluation of methodology's capability to detect the measurable variables and EUs that mostly deviate from health operation and also suits the application to field data, which are by nature unlabeled.

The faulty detection criterion is tuned by setting $k = 3$ and by calculating σ by means of Eq. (7), as the standard deviation of the residuals between the tested healthy data and the corresponding CA predictions. The values of σ employed for applying the fault detection criterion are reported in Table 5.

Table 5
Standard deviation values used for applying the fault detection criterion.

End-user #	Q [kg/s]	p [Pa]	T [°C]
1	3.84E-02	1076	0.51
2	2.45E-02	1036	0.41
3	1.51E-02	814	0.51
4	8.35E-03	77	0.40
5	7.36E-03	681	1.73
6	5.01E-03	677	0.50
7	3.80E-02	154	0.44
8	1.80E-03	79	0.34
9	2.42E-03	73	0.31
10	4.70E-03	398	0.39
11	6.02E-04	69	0.33
12	8.07E-03	1324	0.41

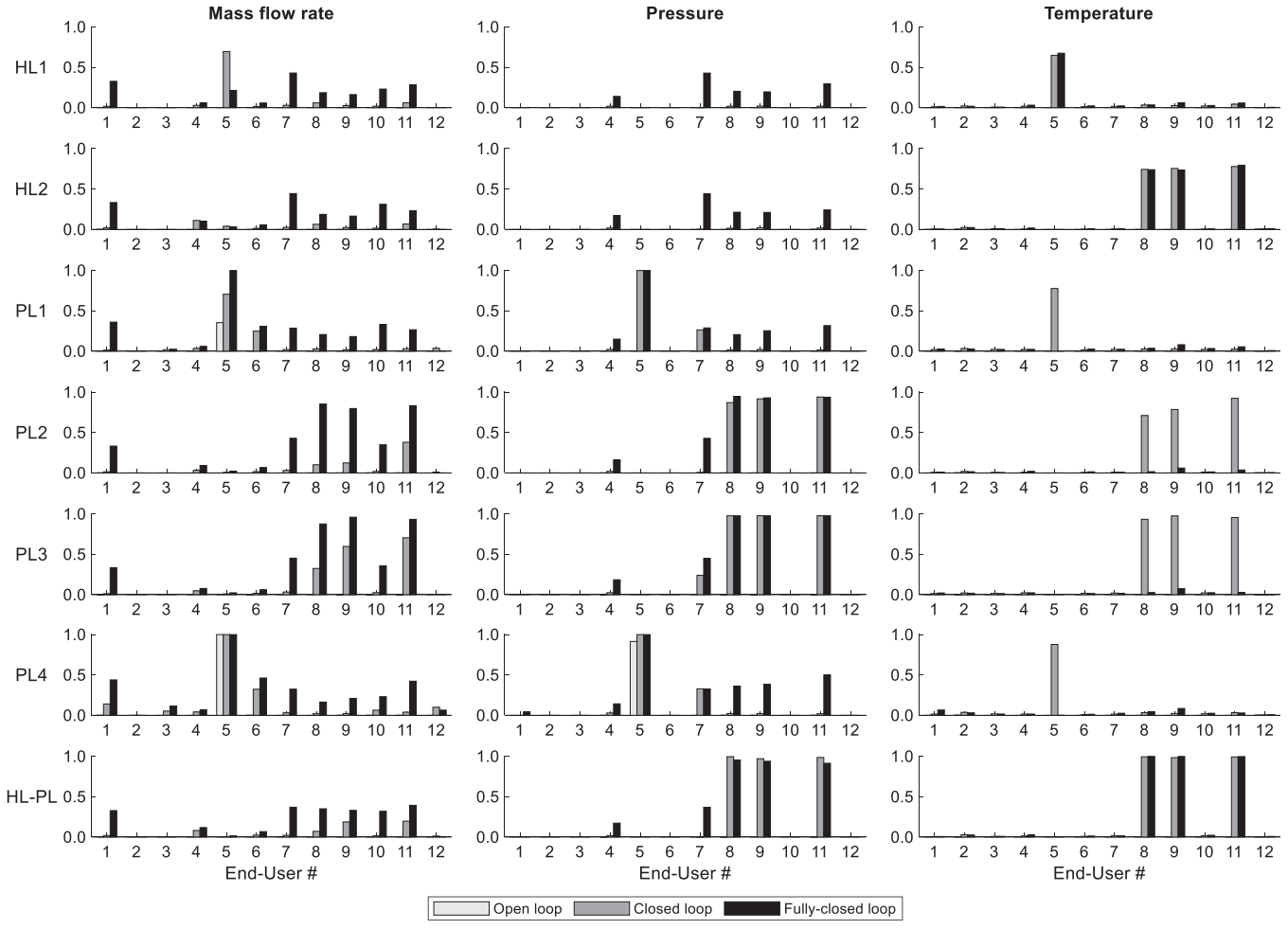

Fig. 7. Detection rate α for the seven faulty datasets.

4.3.1. OA

The results prove that OA provides the lowest reliability since it only allows the detection of fault PL4, by correctly identifying most of the faulty data of Q and p of EU5 (in fact, the detection rate α is higher than 90%), thus also finding the correct fault location. As shown in Fig. 6, fault PL4 can be considered a major fault since the relative change of Q and p of EU5 is close to 5% and 2.5%, respectively. In all the remaining faulty scenarios, the OA provides detection rates close to zero; thus, the diagnostic method cannot detect the implanted faults. The poor reliability of the diagnostic method with OA is related to the use of "true" data of the delayed values (i.e., at past time steps) of the target variable; in fact, "true" data are obviously affected by the implanted faults. In such a manner, model prediction at each time step tends to reproduce the faulty behavior of the DHN. Thus, the residual between the faulty data point and model prediction is low and no alert is triggered by the detection criterion.

4.3.2. CA

In order to avoid that feedback values of the target variable are affected by the implanted fault and thus influence model predictions at future time steps, CA must be employed, since it exploits previously predicted data as the delayed values of the target variables. Thus, once properly initialized, CA allows to reduce the influence of the faulty data on model predictions at future time steps.

In general, it can be observed that CA performs better than OA. In fact, as can be grasped from Fig. 7 and based on the results reported in Section 4.1, CA is capable of detecting all the implanted faults by achieving detection rates approximately equal to 70% in faults HL1 and HL2, and higher than 90% in faults PL1 through PL4 and HL-PL. These promising results are achieved for the EUs impacted by each fault, while detection rates lower than 10% are correctly obtained for the EUs not affected by the faults. This means that fault location is also correctly identified. However, in almost all faulty datasets, a high number of data are labeled as faulty for variables that are not influenced by the fault. As an example, a detection rate equal to 70% is provided for Q of EU5 in fault HL1, which is clearly not affected by the implanted fault (increase of thermal conductivity), as demonstrated in Fig. 6. Similarly, in faults PL1 through PL4 (anomalous pressure losses), the detection rate provided by CA is higher than 80% for T of EUs #8, #9, and #11 (faults PL2 and PL3), and EU5 (faults PL1 and PL4), even though the implanted fault is characterized by an increase of the roughness and decrease of internal diameter. Instead, in fault HL2, faulty data of T are only detected in EUs #8, #9, and #11, as well as, in fault HL-PL (both heat and pressure losses), faulty data of p and T of EUs #8, #9, and #11 are correctly identified with a detection rate higher than 95%. In summary, when CA is employed, the diagnostic method is able to reliably identify fault location, though, in most cases, fault type cannot be recognized.

Such a limitation of CA to return the correct type of fault (in fact, high values of the detection rate must be obtained only for the variables affected by the fault) is due to the exploitation of true data for predictor variables that, in some cases, are indirectly affected by the fault. In fact, as discussed in Section 4.2, even a single fault can affect multiple variables; moreover, multiple faults can occur simultaneously.

4.3.3. FCA

FCA overcomes this drawback of CA since, in addition to the feedback values of the target variable, also its input variables are estimated and thus they are not affected by the fault.

As described in Section 2, the prediction models of Q, p, and T run in parallel and the predicted data points at a given time step of each model are fed back (i) as inputs of the model itself and (ii) as delayed values of the predictor variables of the remaining models. The results reported in Fig. 7 show that FCA and CA allow comparable detection rates for faults HL2 and HL-PL; these two faults are also correctly diagnosed by CA (both fault location and type). Instead, in the remaining faults (5 out of 7), FCA outperforms CA in terms of detection rate. In fault PL1 (EU5) and faults PL2 and PL3 (EUs #8, #9, and #11), the detection rates of FCA are higher (up to 50%) than those of CA for Q.

Moreover, FCA can identify only the variables that are actually impacted by the fault, according to Fig. 6. In fact, in fault HL1, a lower value for the detection rate is provided for Q of EU5 by FCA, with respect to the value obtained by means of CA. Similarly, in faults PL1 through PL4, which mimic anomalous pressure losses, the detection rate for T of all EUs affected by the implanted fault (EU5 for faults PL1 and PL4, and EUs #8, #9, and #11 for faults PL2 and PL3) is almost null, as expected. Thus, these results convey that FCA is the most suitable architecture for the prediction model. However, it has to be highlighted that the diagnostic method employing FCA also provides few faulty data points for EUs not impacted by the implanted fault, e.g., EU1 in all the faulty datasets. This is related to the fact that the FCA approach is fed with previously forecasted values, thus its prediction is more challenged.

To further validate the detection reliability of the diagnostic method, Fig. 8 reports the values of the relative variation, calculated by means of Eq. (11), of the three variables between the faulty value and the corresponding value predicted by means of FCA. The results reported in this Fig. 8 clearly demonstrate that the diagnostic method can actually reproduce the magnitude of both minor faults (faults PL2 and PL3) and major faults (faults HL1, PL4, and HL-PL), since all the values of the relative variation between the faulty data point and FCA prediction are very close to those reported in Fig. 6.

5. Conclusions

The paper developed a data-driven diagnostic methodology to assess the health state of District Heating Networks (DHNs). The novel diagnostic methodology exploited NARX neural networks to predict DHN healthy operation and a threshold-based criterion for fault detection and identification. The DHN of the campus of the University of Parma (Italy), where single and multiple faults of different types and magnitudes were artificially implanted in DHN pipes, was selected as the case study to validate the proposed diagnostic approach.

The methodology comprised two phases. In the first phase, several prediction models were trained on healthy data to mimic the dynamic behavior of a healthy DHN by considering different configurations of the NARX neural network (i.e., delay and number of hidden neurons) and different subsets of data for training and validation. Subsequently, each prediction model was tested on unseen healthy data to assess their prediction reliability and identify the optimally trained model to predict mass flow rate, pressure, and temperature values for each end-user of the DHN. The standard deviation of the residuals between the true values of healthy data and the respective predictions of the optimal prediction models was evaluated to tune the fault detection criterion.

In the second phase, the optimally-trained prediction models were employed for the real-time prediction of the measurable variables of each EU. The fault detection criterion was used to detect DHN faults by comparing the actual data of the DHN to those provided by the prediction model. Seven different faulty datasets characterized by implanted faults mimicking anomalous pressure and temperature losses were investigated.

Three different architectures of the prediction model were tested, namely open-loop, closed-loop, and fully closed-loop, which make use of an increasing amount of self-generated inputs to predict the subsequent data point. The open-loop architecture provided poor detection reliability (only 1 out of 7 faults was correctly detected and isolated). The closed-loop architecture allowed a reduction of the influence of the faulty data on model predictions at future time steps. In fact, the closed-loop architecture was capable of detecting all the implanted faults by achieving detection rates approximately equal to 70% in two faulty datasets, and higher than 90% in the remaining five faulty datasets. However, in most cases, the closed-loop architecture was not capable of recognizing the fault type, since a high number of data were labeled as faulty for variables that were not influenced by the implanted fault.

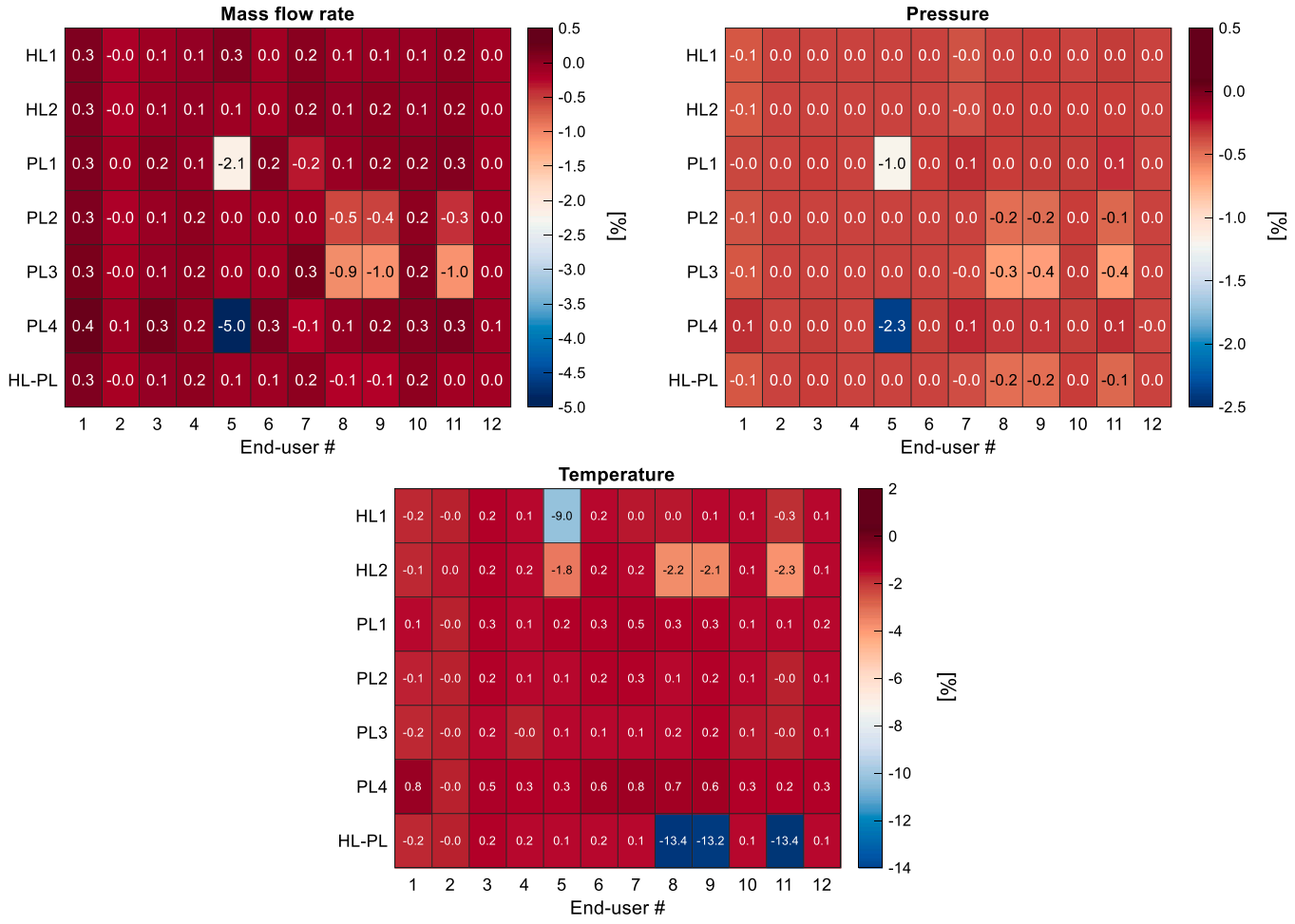

Fig. 8. Relative variation of the three variables due to the implanted faults (faulty value *vs.* value predicted by means of FCA).

Instead, the fully closed-architecture provided comparable or even higher detection rates than closed-loop architecture, but it was also able to identify only the measurable variables that were actually affected by the implanted fault. Moreover, the fully closed-architecture also proved able to correctly reproduce the magnitude of both minor and major faults.

In conclusion, the proposed diagnostic methodology proved general and effective since it could be employed both during steady-state and transient operation. Moreover, the methodology was able to diagnose the considered faults, characterized by different types and magnitudes. Even if in some cases fault magnitude may seem significant, the faults were selected in such a manner that their fault magnitude can be diagnosed, by taking into account the relationship between fault magnitude and the corresponding variation in DHN measurable variables. Finally, thanks to its data-driven nature, it can be potentially applied to all DHNs, regardless of their configuration, size, and age since no piece of information about DHN geometry and characteristics has to be provided.

Future works will be aimed at further validating the methodology, by considering a wider range of boundary conditions. Moreover, a sensitivity analysis will be conducted to identify the fault magnitude that allows its reliable detectability. Finally, an additional analysis will be conducted to evaluate the influence of the available variables on methodology capability, in case of poorly instrumented DHNs.

CRediT authorship contribution statement

Enzo Losi: Writing – review & editing, Writing – original draft, Visualization, Validation, Software, Methodology, Investigation, Formal analysis, Data curation, Conceptualization. **Lucrezia Manservigi:** Writing – review & editing, Writing – original draft, Visualization, Validation, Data curation. **Pier Ruggero Spina:** Writing – review & editing, Visualization, Validation, Supervision, Project administration, Funding acquisition, Data curation, Conceptualization. **Mauro Venturini:** Writing – review & editing, Writing – original draft, Visualization, Validation, Supervision, Data curation, Conceptualization.

Declaration of Competing Interest

The authors declare that they have no known competing financial interests or personal relationships that could have appeared to influence the work reported in this paper.

Data Availability

The data that has been used is confidential.

Acknowledgments

This paper was carried out in the framework of the research program "ENERGYNIUS - ENERGY Networks Integration for Urban Systems (PG/2018/632084)" and the project funded under the National Recovery and Resilience Plan (NRRP), Mission 04 Component 2 Investment 1.5 - NextGenerationEU, Call for tender n. 3277 dated 30/12/2021. Award Number: 0001052 dated 23/06/2022.

Appendix

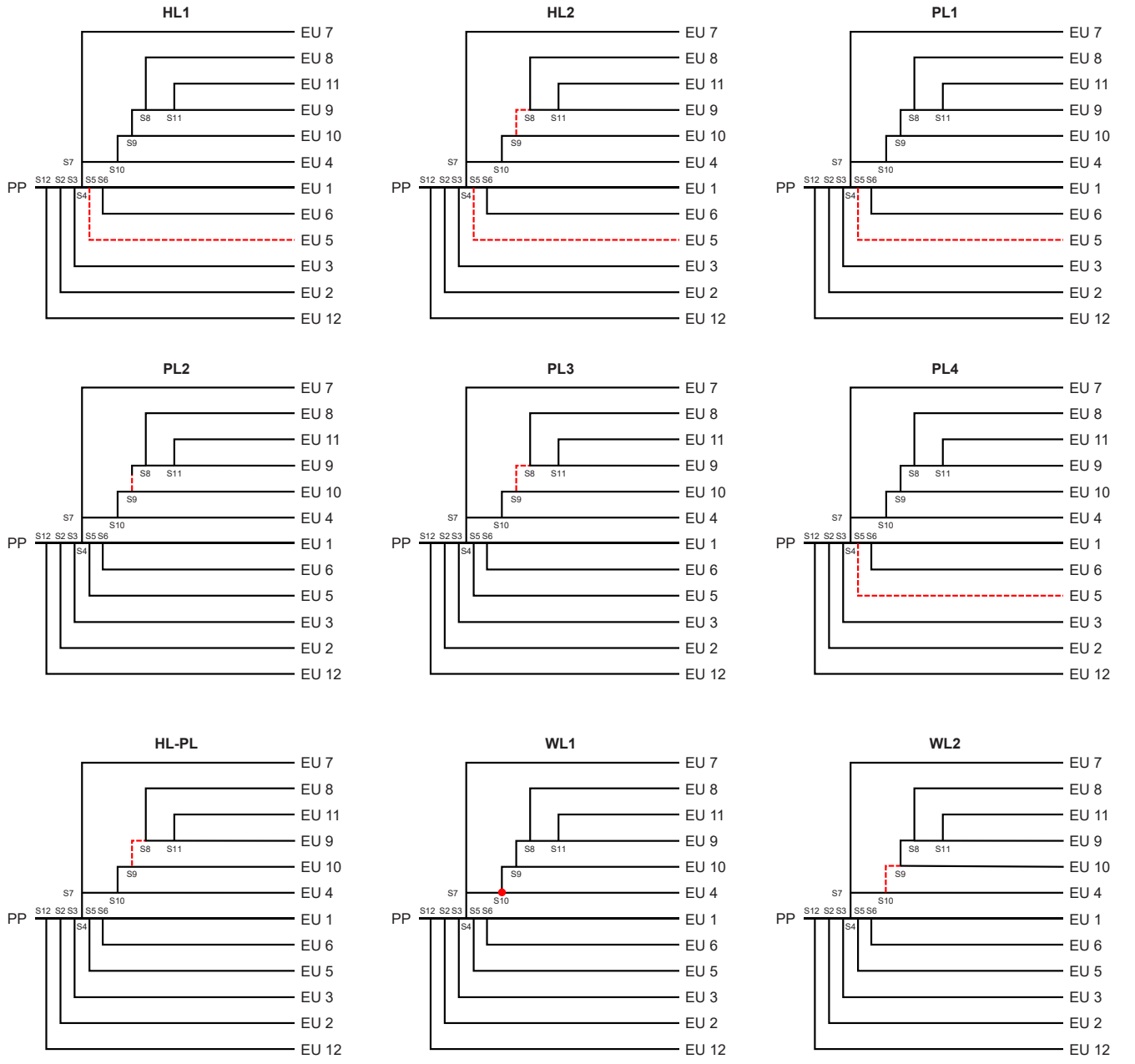

Figure A1. Location of the implanted faults.

References

[1] R.M. Elavarasan, R. Pugazhendhi, M. Irfan, L. Mihet-Popa, I.A. Khan, P. E. Campana, State-of-the-art sustainable approaches for deeper decarbonization in Europe – An endowment to climate neutral vision, Renew. Sustain. Energy Rev. 159 (2022) 112204, https://doi.org/10.1016/j.rser.2022.112204.

[2] A. Franco, M. Versace, Multi-objective optimization for the maximization of the operating share of cogeneration system in District Heating Network, Energy Convers. Manag 139 (2017) 33–44, https://doi.org/10.1016/j.enconman.2017.02.029.

[3] D. Balić, D. Maljković, D. Lončar, Multi-criteria analysis of district heating system operation strategy, Energy Convers. Manag. 144 (2017) 414–428, https://doi.org/10.1016/j.enconman.2017.04.072.

[4] M. Capone, E. Guelpa, V. Verda, Potential for supply temperature reduction of existing district heating substations, Energy 285 (2023) 128597, https://doi.org/10.1016/j.energy.2023.128597.

[5] C. Mateu-Royo, S. Sawalha, A. Mota-Babiloni, J. Navarro-Esbrí, High temperature heat pump integration into district heating network, Energy Convers. Manag 210 (2020) 112719, https://doi.org/10.1016/j.enconman.2020.112719.

[6] D. Mao, P. Wang, W. Wang, L. Ni, Reliability segment design in single-source district heating networks based on valve network models, Sustain Cities Soc. 63 (2020) 102463, https://doi.org/10.1016/j.scs.2020.102463.

[7] X. Shan, P. Wang, W. Lu, The reliability and availability evaluation of repairable district heating networks under changeable external conditions, Appl. Energy 203 (2017) 686–695, https://doi.org/10.1016/j.apenergy.2017.06.081.

[8] P.H. Zou, C.H. Lei, W. Wang, X.M. Bai, J. Yang, District heating networks failure investigation and analysis in Heilongjiang Province, Dist. Heat. 5 (2008) 15–20 ([in Chinese]).

[9] D. Mao, P. Wang, Y. Ju, L. Ni, Failure consequence evaluation of uncontrollable district heating network, Sustain Cities Soc. 78 (2022) 103593, https://doi.org/10.1016/j.scs.2021.103593.

[10] H. Gadd, S. Werner, Fault detection in district heating substations, Appl. Energy 157 (2015) 51–59, https://doi.org/10.1016/j.apenergy.2015.07.061.

[11] S. Buffa, M.H. Fouladfar, G. Franchini, I.L. Gabarre, M.A. Chicote, Advanced control and fault detection strategies for district heating and cooling systems—a review, Appl. Sci. 11 (2021) 455, https://doi.org/10.3390/app11010455.

[12] S. Zhou, Z. O'Neill, C. O'Neill, A review of leakage detection methods for district heating networks, Appl. Therm. Eng. 137 (2018) 567–574, https://doi.org/10.1016/j.applthermaleng.2018.04.010.

[13] Ryunhee K., Yejin H., Youngwoong C., Sungmin Y. System-level fouling detection of district heating substations using virtual-sensor-assisted building automation system. Energy 2021;227-120515. https://doi.org/10.1016/j.energy.2021.120515.

[14] S. Wang, Q. Zhou, F. Xiao, A system-level fault detection and diagnosis strategy for HVAC systems involving sensor faults, Energy Build. 42 (4) (2010) 477–490, https://doi.org/10.1016/j.enbuild.2009.10.017.

[15] D. Gao, S. Wang, K. Shan, C. Yan, A system-level fault detection and diagnosis method for low delta-T syndrome in the complex HVAC systems, Appl. Energy 164 (2016) 1028–1038, https://doi.org/10.1016/j.apenergy.2015.02.025.

[16] E. Davoudi, B. Vaferi, Applying artificial neural networks for systematic estimation of degree of fouling in heat exchangers, Chem. Eng. Res. Des. 130 (2018) 138–153, https://doi.org/10.1016/j.cherd.2017.12.017.

[17] S. Lalot, H. Palsson, Detection of fouling in a cross-flow heat exchanger using a neural network based technique, Int. J. Therm. SciTherm Sci. 49 (4) (2010) 675–679, https://doi.org/10.1016/j.ijthermalsci.2009.10.011.

[18] E. Losi, M. Venturini, L. Manservigi, G.F. Ceschini, G. Bechini, Anomaly detection in gas turbine time series by means of bayesian hierarchical models, J. Eng. Gas. Turbines Power 141 (11) (2019) 111019, https://doi.org/10.1115/1.4044781.

[19] L. Manservigi, M. Venturini, G.F. Ceschini, G. Bechini, E. Losi, Development and validation of a general and robust methodology for the detection and classification of gas turbine sensor faults, J. Eng. Gas. Turbines Power 142 (2) (2020) 021009, https://doi.org/10.1115/1.4045711.

[20] L. Manservigi, D. Murray, J. Artal de la Iglesia, G.F. Ceschini, G. Bechini, E. Losi, Detection of unit of measure inconsistency in gas turbine sensors by means of support vector machine classifier, ISA Trans. 123 (2022) 323–338, https://doi.org/10.1016/j.isatra.2021.05.034.

[21] L. Manservigi, M. Venturini, E. Losi, G. Bechini, J. Artal de la Iglesia, Optimal classifier to detect unit of measure inconsistency in gas turbine sensors, Machines 10 (4) (2022) 228, https://doi.org/10.3390/machines10040228.

[22] P. Xue, Z. Zhou, X. Fang, X. Chen, L. Liu, Y. Liu, J. Liu, Fault detection and operation optimization in district heating substations based on data mining techniques, Appl. Energy 205 (2017) 926–940, https://doi.org/10.1016/j.apenergy.2017.08.035.

[23] M. Li, W. Deng, K. Xiaho, T. Ji, Q. Wu, A data-driven method for fault detection and isolation of the integrated energy-based district heating system, IEEE Access 8 (2020) 23787–23801, https://doi.org/10.1109/ACCESS.2020.2970273.

[24] L. Manservigi, H. Bahlawan, E. Losi, M. Morini, P.R. Spina, M. Venturini, A diagnostic approach for fault detection and identification in district heating networks, Energy 251 (2022) 123988, https://doi.org/10.1016/j.energy.2022.123988.

[25] A. Hlebnikov, A. Volkova, O. Dzuba, A. Poobus, Ü. Kask, Damages of the Tallinn district heating networks and indicative parameters for an estimation of the networks general condition, Sci. J. Riga. Tech. University Environmental Clim. Technol. 5 (2010) 49–55, https://doi.org/10.2478/v10145-010-0034-3.

[26] B. Rüger, D. Pierl, M. Guber, J. Yin, M. Baur, H. Eberhard, F. Klawonn, K. Michels, Online leakage attribution to exclusion areas prototype application, 575-548, Energy Procedia 149 (2018), https://doi.org/10.1016/j.egypro.2018.08.222.

[27] P. Xue, Y. Jiang, Z. Zhou, X. Chen, X. Fang, J. Liu, Machine learning-based leakage fault detection for district heating networks, Energy Build. 223 (2020) 110161, https://doi.org/10.1016/j.enbuild.2020.110161.

[28] Hossain K., Villebro F., Forchhammer S. UAV image analysis for leakage detection in district heating systems using machine learning. Pattern Recogn Lett;140;154-164. https://doi.org/10.1016/j.patrec.2020.05.024.

[29] Q. Fan, Y. Guo, S. Wu, X. Liu, Two-level Diagnosis of Heating Pipe Network Leakage Based on Deep Belief Network, IEEE Access 7 (2019) 182983–182992, https://doi.org/10.1109/ACCESS.2019.2960107.

[30] S. Zhou, C. Liu, Y. Zhao, G. Zhang, Y. Zhang, Leakage diagnosis of heating pipe-network based on BP neural network, Sustain. Energy, Grids Netw. 32 (2022) 100869, https://doi.org/10.1016/j.segan.2022.100869.

[31] M. Nowak-Ocłoń, P. Ocłoń, Thermal and economic analysis of preinsulated and twin-pipe heat network operation, Energy 20 (2020) 116619, https://doi.org/10.1016/j.energy.2019.116619.

[32] S. Chicherin, V. Mašatin, A. Siirde, A. Volkova, Method for assessing heat loss in a district heating network with A focus on the state of insulation and actual demand for useful energy, Energies 13 (17) (2020) 4505, https://doi.org/10.3390/en13174505.

[33] J. Danielewicz, B. Śniechowska, M.A. Sayegh, N. Fidorów, H. Jouhara, Three-dimensional numerical model of heat losses from district heating network pre-insulated pipes buried in the ground, Energy 180 (2016) 172–184, https://doi.org/10.1016/j.energy.2015.07.012.

[34] X. Zheng, Q. Sun, Y. Wang, L. Zheng, X. Gao, S. You, H. Zhang, K. Shi, Thermo-hydraulic coupled simulation and analysis of a real largescale complex district heating network in Tianjin, Energy 236 (2021) 121389, https://doi.org/10.1016/j.energy.2021.121389.

[35] T. Fang, R. Lahdelma, State estimation of district heating network based on customer measurements, Appl. Therm. Eng. 73 (2014) 1211–1221, https://doi.org/10.1016/j.applthermaleng.2014.09.003.

[36] P. Lidén, B. Adl-Zarrabi, C.E. Hagentoft, Diagnostic protocol for thermal performance of district heating pipes in operation. Part 1: estimation of supply pipe temperature by measuring temperature at valves after shutdown, Energies 14 (16) (2021) 5192, https://doi.org/10.3390/en14165192.

[37] P. Lidén, B. Adl-Zarrabi, C.E. Hagentoft, Diagnostic protocol for thermal performance of district heating pipes in operation. Part 2: estimation of supply pipe temperature by measuring temperature at valves after shutdown, Energies 14 (2021) 5302, https://doi.org/10.3390/en14175302.

[38] H. Wang, H. Meng, T. Zhu, New model for onsite heat loss state estimation of general district heating network with hourly measurements, Energy Convers. Manag 157 (2018) 71–85, https://doi.org/10.1016/j.enconman.2017.11.062.

[39] A. Keçebaş, I. Yabanova, Thermal monitoring and optimization of geothermal district heating systems using artificial neural network: a case study, Energy Build. 50 (2012) 339–346, https://doi.org/10.1016/j.enbuild.2012.04.002.

[40] Kaltenbacher S., Steinberger M., Horn M. Applied Pipe Roughness Identification of Water Networks: Consideration of All Flow Regimes. IEEE Transactions on Control Systems Technology 2022. https://doi.org/10.1109/TCST.2022.3193786.

[41] H. Bahlawan, N. Ferraro, A. Gambarotta, E. Losi, L. Manservigi, M. Morini, C. Saletti, P.R. Spina, M. Venturini, Detection and identification of faults in a district heating network, Energy Convers. Manag 266 (2022) 115837, https://doi.org/10.1016/j.enconman.2022.115837.

[42] Bahlawan H., Gambarotta A., Losi E., Manservigi L., Morini M., Saletti C., Spina P. R., Venturini V. Fault diagnosis in district heating networks. J Phys: Conf Ser 2385 012096. https://doi.org/10.1088/1742-6596/2385/1/012096.

[43] D. Romanchenko, J. Kensby, M. Odenberger, F. Johnsson, Thermal energy storage in district heating: centralised storage vs. storage in thermal inertia of buildings, Energy Convers. Manag 162 (2018) 26–38, https://doi.org/10.1016/j.enconman.2018.01.068.

[44] B. Sdiri, L. Rigaud, R. Jemmali, et al., The difficult path to become data-driven, SN Comput. Sci. 4 (2023) 385, https://doi.org/10.1007/s42979-023-01789-y.

[45] E. Losi, M. Venturini, and, L. Manservigi, Gas turbine health state prognostics by means of bayesian hierarchical models. ASME, J. Eng. Gas. Turbines Power 141 (11) (November 2019) 111018, https://doi.org/10.1115/1.4044689.

[46] E. Losi, M. Venturini, L. Manservigi, and, G. Bechini, Detection of the onset of trip symptoms embedded in gas turbine operating data. ASME, J. Eng. Gas. Turbines Power 145 (3) (March 2023) 031023, https://doi.org/10.1115/1.4055904.

[47] G. Bode, S. Thul, M. Baranski, D. Müller, Real-world application of machine-learning-based fault detection trained with experimental data, Energy 198 (2020) 117323, https://doi.org/10.1016/j.energy.2020.117323.

[48] J. van Dreven, V. Boeva, S. Abghari, H. Grahn, J. Al Koussa, E. Motoasca, Intelligent approaches to fault detection and diagnosis in district heating: current trends, challenges, and opportunities, Electronics 12 (6) (2023) 1448, https://doi.org/10.3390/electronics12061448.

[49] M. Neumayer, D. Stecher, S. Grimm, A. Maier, D. Bücker, J. Schmidt, Fault and anomaly detection in district heating substations: a survey on methodology and data sets, Energy 276 (2023) 127569, https://doi.org/10.1016/j.energy.2023.127569.

[50] M. Vallee, T. Wissocq, Y. Gaoua, N. Lamaison, Generation and evaluation of a synthetic dataset to improve fault detection in district heating and cooling systems, Energy 283 (2023) 128387, https://doi.org/10.1016/j.energy.2023.128387.

[51] R. Berntsson Svensson, M. Taghavianfar, Toward Becoming a Data-Driven Organization: Challenges and Benefits, in: F. Dalpiaz, J. Zdravkovic, P. Loucopoulos (Eds.), Research Challenges in Information Science. RCIS 2020. Lecture Notes in Business Information Processing, vol 385, Springer, Cham, 2020, https://doi.org/10.1007/978-3-030-50316-1_1.

[52] R. Kim, Y. Hong, Y. Choi, S. Yoon, System-level fouling detection of district heating substations using virtual-sensor-assisted building automation system, Energy 227 (2021) 120515.

[53] Park, S., Moon, J., Hwang, E. Explainable Anomaly Detection for District Heating Based on Shapley Additive Explanations. In Proceedings of the 2020 International Conference on Data Mining Workshops (ICDMW), Virtual, 17–20 November 2020; pp. 762–765.

[54] M. Bai, J. Liu, J. Chai, X. Zhao, D. Yu, Anomaly detection of gas turbines based on normal pattern extraction, Appl. Therm. Eng. 166 (2020) (2020) 114664.

[55] M.A. Ancona, L. Branchini, A. De Lorenzi, A. De Pascale, A. Gambarotta, F. Melino, M. Morini, Application of different modeling approaches to a district heating network, AIP Conf. Proc. 2191 (2019) 020009, https://doi.org/10.1063/1.5138742.

[56] A. De Lorenzi, A. Gambarotta, M. Morini, M. Rossi, C. Saletti, Setup and testing of smart controllers for small-scale district heating networks: an integrated framework, Energy 205 (2020) 118054, https://doi.org/10.1016/j.energy.2020.118054.

[57] S. Månsson, I. Lundholm Benzi, M. Thern, R. Salenbien, K. Sernhed, P.O. Johansson Kallioniem, A taxonomy for labeling deviations in district heating customer data, Smart Energy 2 (2021) 100020.